Lake-Effect Rain Events

TODD J. MINER AND J. M. FRITSCH

Department of Meteorology, The Pennsylvania State University, University Park, Pennsylvania

(Manuscript received 2 July 1996, in final form 18 April 1997)

ABSTRACT

Seven years of autumnal (September–November) precipitation data are examined to determine the characteristics of lake-effect precipitation downwind of Lake Erie. Atmospheric conditions for each lake-effect event are compiled and the mean atmospheric environment for rain events is constructed and compared to conditions for lake-effect snow events.

It is found that lake-effect precipitation occurs approximately one out of every five days with a diurnal peak in precipitation intensity during the afternoon and evening. The greatest number of lake-effect days occurs in October followed by November and then September. Comparison of these results to regional precipitation climatologies strongly suggests that the season of lake enhanced precipitation begins in late summer. Precipitation is predominantly rain throughout September and October and snow after the first week of November. A transition period of both rain and snow occurs in early November. Analysis of thunder events for the 7-yr period show a late September to mid-October peak with a decline in frequency by November. The decline in thunder events is due to a seasonal decrease in the depth of the conditionally unstable layer.

As might be expected, the mean atmospheric conditions during rain events are similar to those found during lake-effect snow events. This is particularly true with regard to the overall positions of transient synoptic features. Differences are most apparent in the thermodynamic profile of the lower troposphere. Extreme low-level instabilities typically observed in lake-effect snow events are absent from lake-effect rain events. However, in contrast to most snow events, a much deeper layer of conditionally unstable air is usually present during rain events.

1. Introduction

Both the theoretical and operational meteorological communities have produced a significant amount of literature documenting the many aspects of lake-effect snows. Wiggin (1950) pioneered the operational forecast practices for lake-effect snow in Western New York. Since then, the works of Holroyd (1971), Kolker (1978), Dockus (1985), Niziol (1987 et al. 1995) and others have greatly improved the predictability of these mesoscale snow events. At the same time, theoretical research and modeling studies (eg., Hill 1971; Lavoie 1972; Lenschow 1973; Hjelmfelt 1990; Byrd et al. 1991; Ballentine et al. 1993; Sousounis and Fritsch 1994) have increased the understanding of how individual lakes contribute to local episodes of lake-effect snow as well as how the lakes act as an aggregate to enhance regional snowfall. In contrast, relatively little attention has been given to the beginning of the fall season when early cold-air outbreaks over the warm lakes can generate lake-effect rains. Although some studies have documented such events (e.g., Changnon and Jones 1972; Changnon 1988; Moore and Orville 1990; Mundshenck 1993), a more comprehensive investigation of this phenomenon is needed.

Climatological data suggest that the ''unstable'' portion of the lake-effect season downwind of Lake Erie commences well before the first snow occurs. For example, the potential for lake-effect is readily apparent from a comparison (Fig. 1) of the seasonal distribution of mean Lake Erie temperature to the air temperature at Buffalo, New York, a nearby reporting station. The Lake Erie temperature exceeds the Buffalo air temperature from midsummer through the end of winter. This period is considered the ''unstable'' portion of the lake-effect season during which Lake Erie climatologically enhances downwind cloudiness and precipitation. By early spring, the pattern reverses with the average Lake Erie temperature turning cooler than the mean Buffalo air temperature. Note that the magnitude of the temperature difference during the ''unstable season'' is greatest from late fall to late winter.

To examine the effect of this temperature difference on the seasonal distribution of downstream precipitation, the mean monthly precipitation for an area immediately downwind of Lake Erie was compared to the average of 36 locations well away from Lake Erie but within 700 km of Buffalo, New York (Fig. 2). The results of the comparison (Fig. 3) show that large differ-

Corresponding author address: Todd J. Miner, Department of Meteorology, The Pennsylvania State University, 503 Walker Bldg., University Park, PA 16802-5013.
E-mail: miner@psumeteo.psu.edu

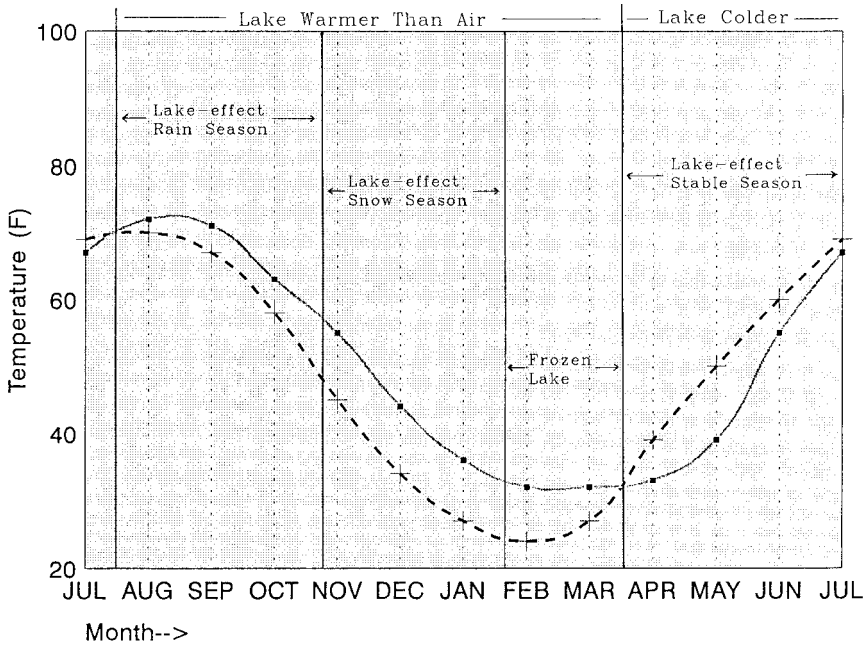

FIG. 1. Annual cycle of mean air (dashed) and mean Lake Erie temperature (solid) at Buffalo, New York. Lake-effect stable and unstable seasons are highlighted downwind of Lake Erie based on the sign of the air–lake temperature difference (NWS Buffalo, New York 1987)

ences in climatological precipitation commence in August (about the time the mean lake temperature exceeds the mean Buffalo temperature). A similar result was found for the area immediately downstream of Lake Ontario.[1] Because these stations lie in the same climatological region, the observed precipitation differences are likely induced by Lake Erie and Ontario. The maximum precipitation contribution from Lake Erie appears to occur in November. Significant precipitation differences are noted, however, from August through December.[2]

The purpose of this paper is to document the frequency and magnitude of autumnal Lake Erie–effect precipitation events as well as the atmospheric conditions most likely to produce them. The following section describes the data and methodology used in the analyses. Sections 3 and 4 present the results and a brief comparison between the environment of lake-effect rain and lake-effect snow events. The final section summarizes the results and offers some concluding remarks.

[1] Note that even though these ''non-lake-effect stations'' are hundreds of kilometers from the lakes, they likely receive some lake-effect precipitation. Thus the results presented in Fig. 3 can be considered a conservative estimate of the lake effect.

[2] The small positive values of the spring and early summer (Fig. 3) suggest that Lake Erie's role in reducing precipitation during the stable season may be confined to local corridors downwind of Lake Erie often referred to as the ''lake shadow.'' Convergence along the lake shadow boundary enhances precipitation for some stations in the Lake Erie region, likely contributing to the positive values of spring and early summer.

2. Data and methodology

a. Data

The following data were used in the investigation:

1) standard surface (SAO) and upper-air,
2) cooperative-station daily and monthly precipitation,
3) mixed-layer lake temperature in Buffalo harbor,
4) National Weather Service (NWS) manually digitized radar (MDR) charts,
5) Nested Grid Model (NGM) data, and
6) National Weather Service observed lifted index charts.

Items 1, 4, 5, and 6 were obtained from The Pennsylvania State University Department of Meteorology data archives with some supplementing of upper-air data from the National Center for Atmospheric Research. Item 2 was obtained from the National Climate Data Center while the data in item 3 was obtained from the NWS at Buffalo. A 7-yr period, 1988–94 inclusive, was selected for examination. Because the focus of the study is on early season lake-effect precipitation, specifically rain, the dataset was limited to the months of September through November.

b. Definitions

For the purposes of this investigation, a lake-effect precipitation event is considered to have occurred when the following conditions have been met:

1) a precipitation echo (as detected by NWS composite

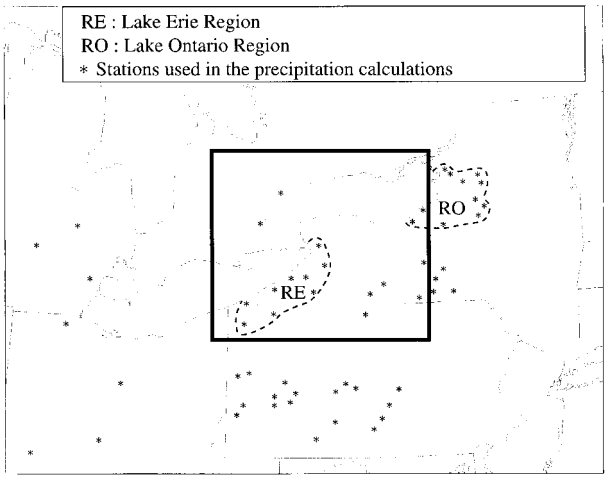

FIG. 2. Asterisks depict the stations used in the mean monthly precipitation calculations. Sites strongly influenced by Lake Erie and Ontario are enclosed in areas labeled RE and RO, respectively. Sites not strongly affected by Lakes Erie or Ontario are located outside these labeled regions. The 400 km × 400 km box used for detecting precipitation echoes for Lake Erie–effect events is also shown.

radar) is observed over or downwind of Lake Erie, within a 400 km × 400 km box centered on Buffalo, New York (see Fig. 2).[3]

2) the echo persists for at least six consecutive hours while lower-tropospheric cold advection (diagnosed by the NGM 00-h surface pressure and 1000–500-mb thickness analyses)[4] is occurring.
3) the lake-surface to 850-mb lapse rate, defined by the lake temperature at Buffalo minus the observed 850-mb Buffalo sounding temperature, exceeds the moist adiabatic rate for the duration of the precipitation echo, and
4) the majority of the precipitation echo's life occurs during cold advection.

Since most *non-lake-effect* precipitation events occur during times of warm advection, restrictions 2 and 4 help eliminate events that are not induced by Lake Erie. The 6-h time requirement helps exclude precipitation events of time and spatial scales of individual convective cloud elements. Last, the moist adiabatic lapse rate restriction ensures that the precipitation events were convectively driven.

Once a lake-effect event is identified, its life cycle is divided into three stages: initial, maximum intensity, and ending. These stages are defined in the following manner:

- initial: first precipitation echo is detected,
- maximum intensity: maximum echo height is observed, and
- ending: last echo of the event is detected.

From these definitions, it follows that the duration of an event is given by the time interval between the initial and ending times. If an MDR chart is missing, precipitation is assumed to be occurring at that time provided precipitation is observed at the hours prior to and after the missing hour. If two or more consecutive hours are missing, the event is excluded, unless precipitation is observed by one of the SAO reporting sites downwind of Lake Erie.

Events are also stratified according to precipitation type, occurrence of heavy rain, and occurrence of thunder. Two precipitation type categories were defined: rain and snow. A rain (snow) event occurred if the precipitation-type was mostly rain (snow) for the duration of the event (as depicted on a NWS MDR composite chart). Thunder events were defined as those that depict ''TRW'' on the MDR composite, while heavy rain events were limited to those in which Buffalo or Erie reported 0.50 in. or more of rain.[5] Hereafter, the term ''lake-effect'' will always refer to Lake Erie–effect precipitation unless otherwise noted.

c. Analysis techniques

Two objective analysis techniques were applied to the standard data for the lake-effect rain events. First, following Hirschberg and Fritsch (1991), sounding data were vertically interpolated from 1000 to 100 mb in 25-mb increments. Temperatures were interpolated logarithmically with pressure; heights were calculated using virtual temperature in the hypsometric equation; and winds and dewpoints were interpolated linearly with height. The program performs several internal error checks to flag inconsistencies in data interpolation. Of the total 64 event times, 13 were flagged for poor wind observations. Although these poor wind events were excluded from wind and wind-derived analysis fields (such as divergence), they were retained for the non-wind-related data analyses such as temperature, dewpoint, heights, and potential temperature.

Surface and upper-level analyses were performed with the Barnes objective analysis technique (Barnes 1964). The radius of influence and corresponding gamma parameter selected for the upper-air analyses were

[3] Due to the poor radar coverage over northwestern Pennsylvania, some of the shallower-topped convective events might not have been detected in the MDR radar summaries. Thus, the total events counted could be a conservative estimate of the actual number.

[4] Because the 00-h NGM analysis is produced only twice daily, there was often a need to estimate the sign of temperature advection between the 0000 and 1200 UTC run times. The estimating was done by visually interpolating the advection-type between the 0000 and 1200 UTC products.

[5] Due to the scarcity of cooperative sites upwind of Lake Erie, the criterion for selecting the heavy rain events did not incorporate rainfall data from cooperative sites downwind of Lake Erie. If this were done, a statistical bias would have been introduced resulting in an unreasonable difference between the upwind and downwind sites.

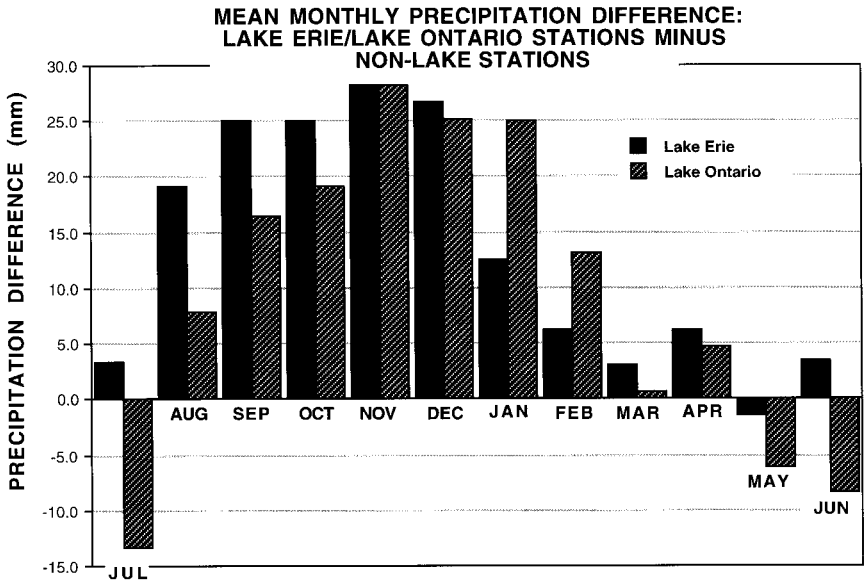

FIG. 3. Annual cycle of mean monthly precipitation differences between stations in the Lake Erie and Ontario regions and the average of all stations outside of these regions. Maximum differences are noted from late summer through early winter.

1000 km and 0.35, respectively. For surface data, different sets of radii and gamma parameters were chosen for each of the two different size map background projections: 750 km and 0.35 for the larger map and 400 km and 0.35 for the smaller.

After applying the objective analysis techniques to the total sample of rain events, an arithmetic mean of the conditions for each of the three stages (initial, maximum intensity, ending) and for thunder events was constructed. Since upper-air data are only available at 0000 and 1200 UTC, just those objectively analyzed fields in which the stratification criteria were valid within 2 h of 0000 or 1200 UTC (sounding times) were used. Table 1 presents the number of rain events that compose the mean surface and upper-air analyses of the three lifecycle stages and thunder events.

3. Results

a. Climatology

1) SEASONAL CHARACTERISTICS

To illustrate the anomalous frequency of cold-advection precipitation downwind of Lake Erie, a tally of cold-advection precipitation events for three regions outside of the Great Lakes (see Fig. 4) was compared to the number of cold-advection events in the Great Lakes region (Fig. 5) for the seven autumns between 1988 and 1994. The comparison indicates a maximum of cold advection precipitation events of all durations in the Great Lakes region. It is hypothesized that this maximum in activity is attributed primarily to the presence of Lake Erie.

The autumnal distribution of total lake-effect precipitation days downwind of Lake Erie is shown in Fig. 6. The values are given in 10-day bins from 1 September

TABLE 1. Number of rain events contained in the mean analyses. The number in parentheses indicates the number of events contained in the wind or wind-derived analyses.

Analysis time	Number of events
Initial	16 (14)
Maximum intensity	16 (12)
Ending	12 (8)
Thunder	20 (17)

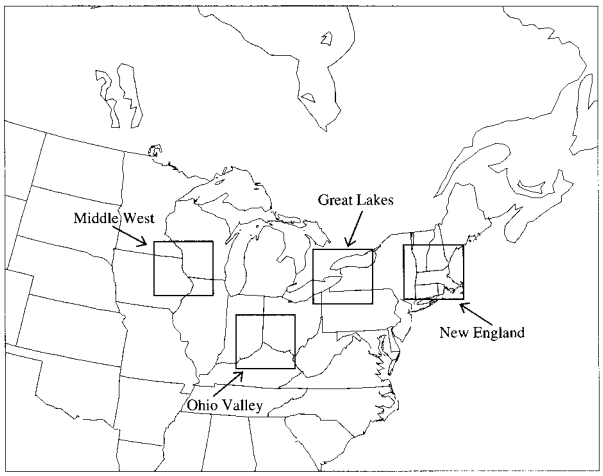

FIG. 4. Boxed regions (400 km × 400 km) where cold advection events were tallied for the seven autumns between 1988 and 1994 (see figure labels).

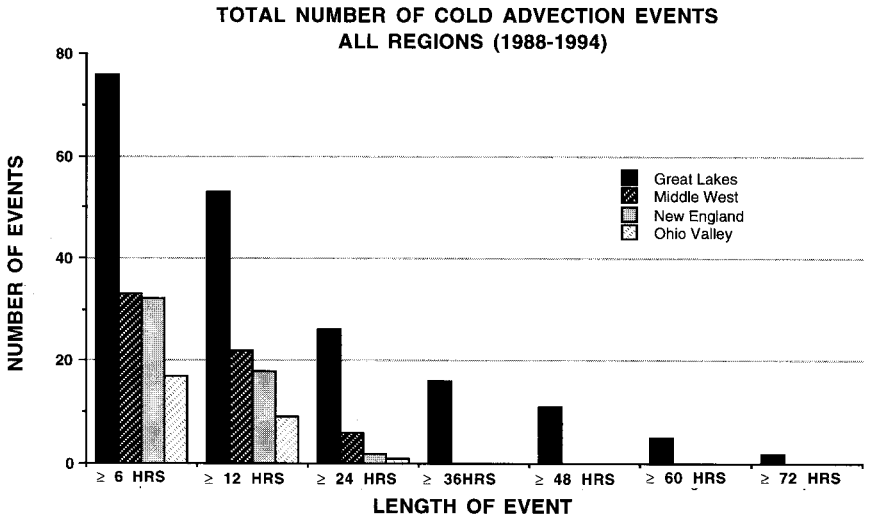

FIG. 5. The number of autumnal cold advection precipitation events in the Great Lakes box and three other nonlake regions (1988–94). Event durations are plotted along the figure bottom.

to 30 November.[6] The lake effect is shown to rapidly increase near the end of September, reaching a peak in early to mid October. The frequencies then decrease slightly into early November followed by another increase in activity toward the end of that month. A notable characteristic of Fig. 6 is the relatively quick transition from lake-effect rain to lake-effect snow days.

In the seven years studied, a total of 32 lake-effect rain events were tallied and 20 snow events were counted. Figure 7 compares the number of lake-effect days to the number of lake-effect events for each month. Since lake-effect events usually span more than one day, the number of lake-effect days exceeds the number of lake-effect events. Tallying the number of lake-effect hours for each month yields areal lake-effect precipitation frequencies of 10%, 24%, and 23% for September, October, and November, respectively. Because large differences exist between areal and point precipitation frequencies (Beebe 1952), the above values would be much lower for any given point within the Lake Erie box (see Fig. 2).

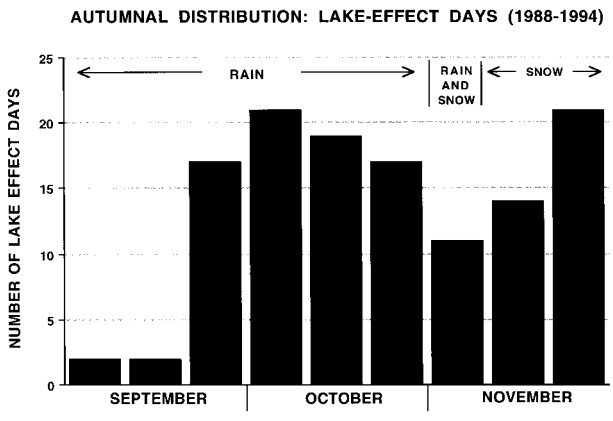

FIG. 6. Distribution of total lake-effect precipitation days in 10-day bins, 1988–94. Predominant precipitation types are indicated at the top of the figure.

[6]Note that the last bin in October contains 11 days since there are 31 days in this month.

Figure 8 shows that heavy lake-effect precipitation occurs in all three autumn months with an apparent maximum from late September to early October. The greatest precipitation event total was 99.8 mm at Sherman, New York, between 3 and 13 October 1988.[7] Lake-effect thunder was also observed in all three months and was most frequent in September and October (Fig. 9). While October tallied the greatest number of lake-effect thunder days, September had the highest proportion of its lake-effect days that produced thunder (over 40%). Not surprisingly, a plot of maximum echo tops and lifted indices (at Buffalo) versus date (Fig. 10) suggest that the seasonal decline in thunder events is related to a seasonal increase in stability. Linear regression analyses show that 20% and 21% of the lifted index and maximum echo top variance, respectively, is explained by its date of occurrence.

2) DIURNAL CHARACTERISTICS

The diurnal distribution of maximum radar echo tops and thunderstorm frequency for all events is shown in Fig. 11. The early evening (0000–0500 UTC) had the greatest tally of maximum radar echo tops while the

[7] Two heavy lake-effect rain events occurred on 14 and 15 September 1996 that were not included in this study. These events produced about 150 mm of rain in Tonawanda, New York, a nearby suburb of Buffalo.

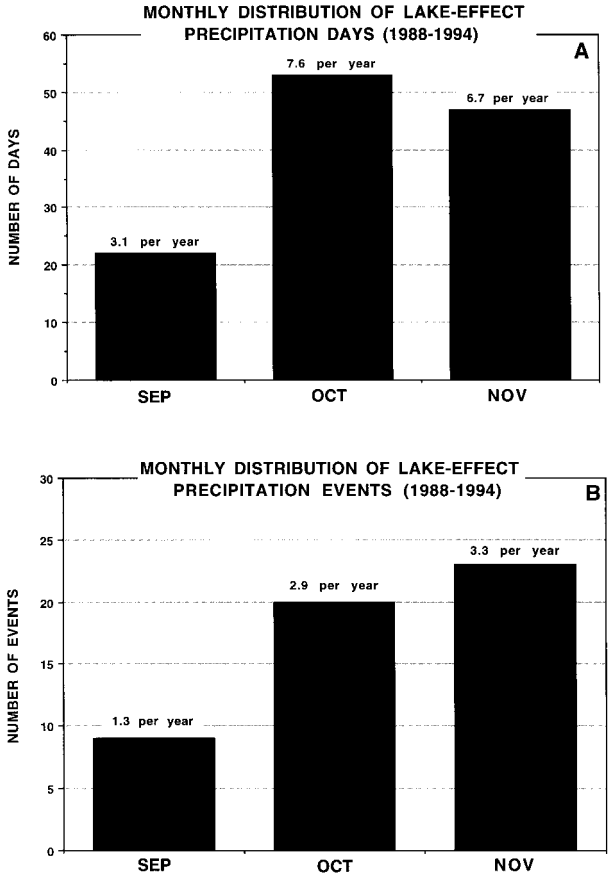

FIG. 7. Monthly distribution of lake-effect days for the years 1988–94. Numbers above each month indicate the average number of lake-effect days per year for that month. (b) Same as (a) but for lake-effect events.

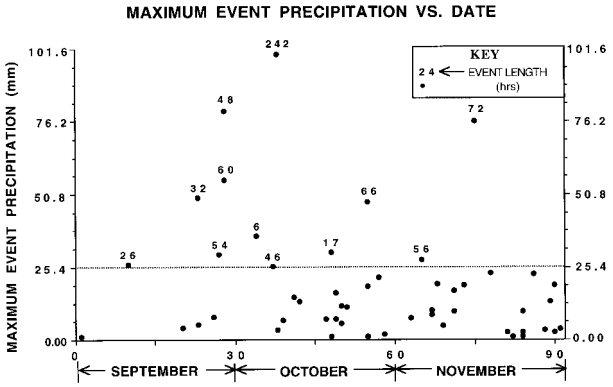

FIG. 8. Maximum event precipitation for stations downward of Lake Erie versus date for all events. Event duration is plotted for those events where precipitation exceeded 25.4 mm.

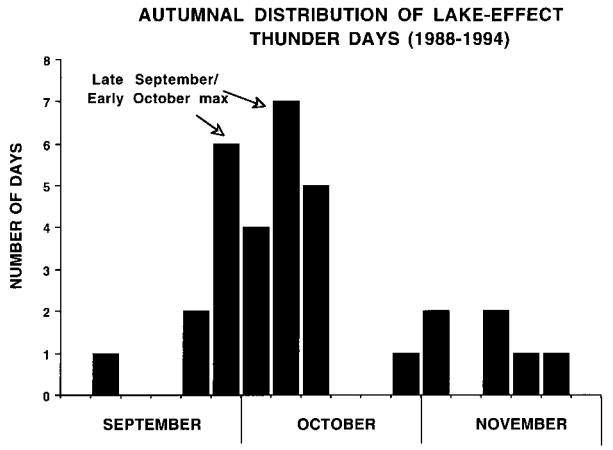

FIG. 9. Seasonal distribution of lake-effect thunder days in 5-day bins between 1988 and 1994.

overnight period between 0600 and 1100 UTC had the fewest. The 0600–1100 UTC overnight minimum was also observed in the occurrences of thunder. In addition, the histogram in Fig. 12 shows that for the nine heavy rain events, the cumulative precipitation for the downwind sites of Erie and Buffalo was greatest during the afternoon and evening (1800 to 0600 UTC) with amounts dropping considerably after 0600 UTC. In contrast, the cumulative precipitation at the upwind sites' histogram has only a daytime maximum and a notable evening to overnight minimum (same figure). This suggests that there is a tendency for autumnal lake-effect rain events to achieve their greatest intensity from late afternoon into the early evening.[8]

The afternoon into early evening peak in activity and overnight decline suggest that boundary layer destabilization is accomplished from both land-based solar heating and overlake heating and moistening. Because the residency time (and subsequent boundary layer destabilization) of air over the lake is often short, the input of upstream land-based heating may be required in some cases to cause convection. At night, in the absence of solar heating, the instability mechanism shifts exclusively to the lake.[9]

b. Mean Buffalo soundings

A mean sounding for lake-effect rain events was produced at Buffalo, New York, for each of the life-cycle stages and for those events where thunder was observed.

[8] The precipitation results should be viewed with some caution due to the relatively small sample of nine heavy rain events.

[9] Environmental regimes likely exist where solar heating is detrimental to lake-effect precipitation. These situations probably occur when very large temperature contrasts between the lake and land produce thermally driven roll vortices (Kelly 1984). Since the intensities of these roll vortices depend upon the maintenance of the differential land/lake heating rates, introducing boundary layer heating over land could cause the thermally induced circulations to weaken (Passarelli and Braham 1981).

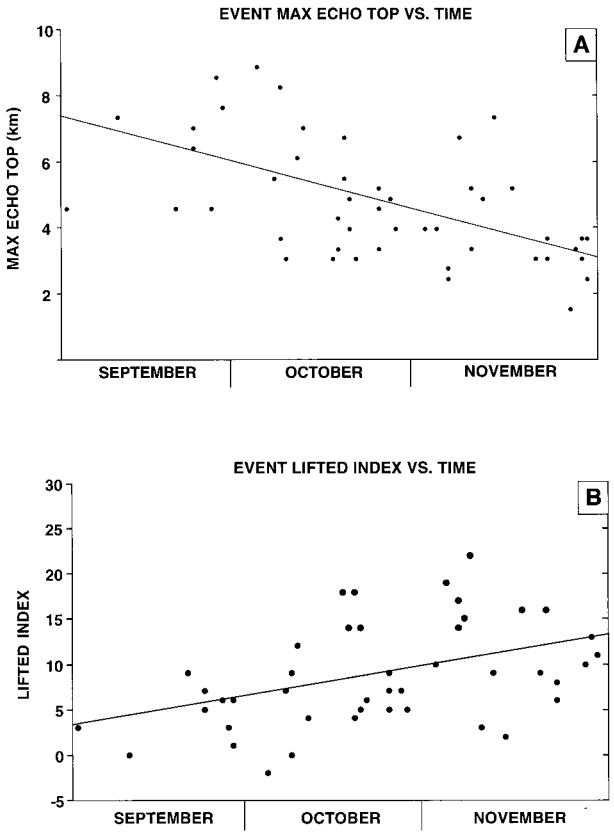

FIG. 10. (a) Maximum echo top vs date for all autumnal lake-effect events (1988–94). Line shows linear regression best fit. (b) Same as (a) but for lifted index. Both (a) and (b) indicate a seasonal trend toward increasing stability.

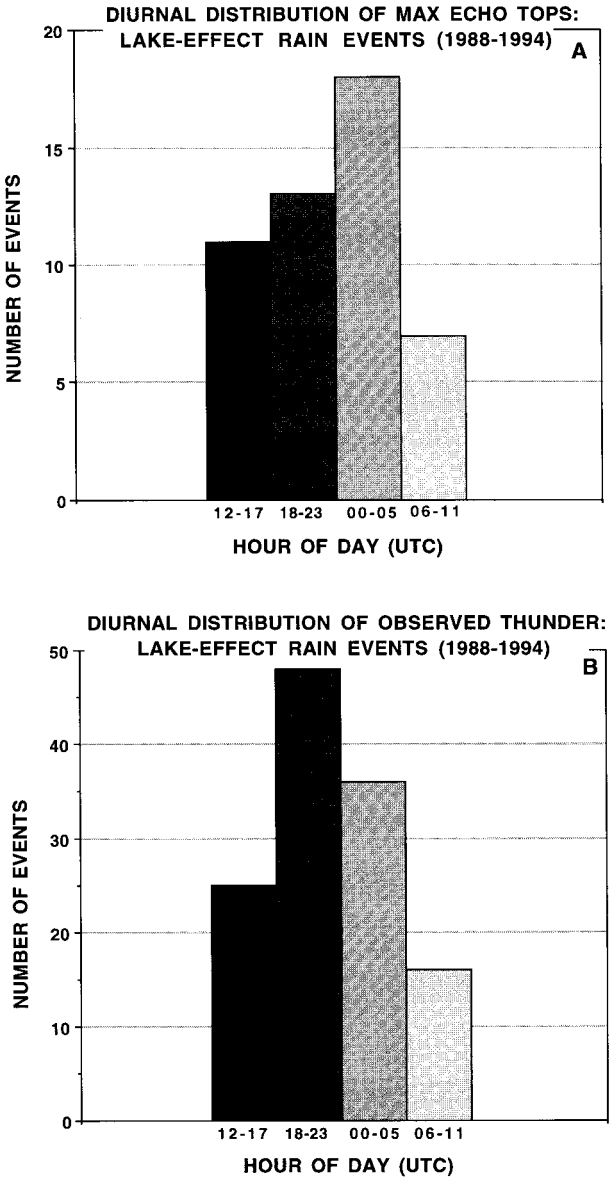

FIG. 11. (a) Diurnal distribution of maximum echo tops for lake-effect rain events. (b) Same as (a) except for thunder observations.

The surface boundary conditions for these soundings were then modified in an attempt to reproduce the thermodynamic profile over Lake Erie.

Prior to modification, the mean initial-stage sounding shows a nearly moist adiabatic environment from the surface through 750 mb (Fig. 13a) with a small inversion detected near 700 mb. This is likely a frontal inversion since, as will be shown later, a large fraction of the initial stage events occurred shortly after cold frontal passage. Application of the National Weather Service's SHARP program Hart and Korotky (1991) to the initial sounding generates lifted index (LI) and convective available potential energy (CAPE) values of 7° and 0 J kg^{-1}, respectively, values atypical of convectively driven precipitation.

Also noted is the minimal directional shear throughout the troposphere with winds uniform from the southwest. A slight backing is observed above 700 mb, indicating the presence of cold advection. Although the directional shear is quite weak, substantial speed shear is evident with speeds increasing from 5 m s^{-1} at the surface to over 40 m s^{-1} near 300 mb. The strong increase in wind speed with height indicates the presence of considerable synoptic-scale baroclinicity. This wind profile is consistent with those observed during intense lake-effect snow events (Niziol 1987) downwind of Lake Erie and Ontario.

The thermodynamic profile observed in the ending stage (Fig. 13a) differs substantially from the initial sounding. Static stabilities have increased significantly (lifted index rose from 7° to 11°), although a shallow layer of nearly moist adiabatic air still exists below 850 mb. Above this shallow moist adiabatic layer, significant drying has occurred. This profile is characteristic of synoptic-scale subsidence. Tropospheric winds have turned to the west and northwest while the slight veering below 600mb indicates that the environment has shifted from cold to warm advection.

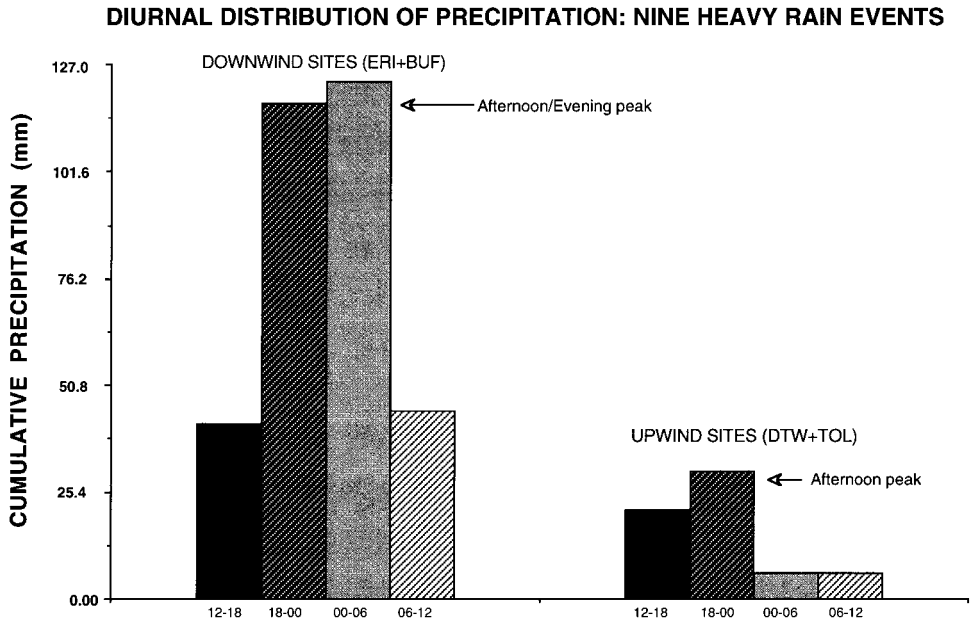

FIG. 12. Diurnal distribution of cumulative precipitation for the nine heavy rain events (mm). Left-hand side depicts the combined rainfall for downwind sites (Erie and Buffalo), while the right-hand side shows the combined rainfall for the upwind sites.

As expected, the mean soundings for the maximum intensity stage and for events with thunder (Fig. 13b) display a more moist (higher relative humidity) and unstable environment than the initial and endings stages. Of particular significance is the near absence of a mid-level inversion. Nonetheless, the lifted indices are still positive and the CAPE still negligible ($+4°/0$ J kg^{-1} and $+3°/6$ J kg^{-1} for the maximum intensity and thunder soundings, respectively). Like the initial sounding, the maximum intensity and thunder soundings show very little directional shear with west to southwesterly flow.

c. *Modified soundings*

The lack of convective instability in the four sounding profiles calls into question the convective nature of these events. After all, parcel theory requires that at least some buoyant energy (CAPE) be present to initiate convective precipitation. Since the mean thunder sounding comprises 19 occasions in which thunder was observed, it is undeniable that deep convection occurred in many of

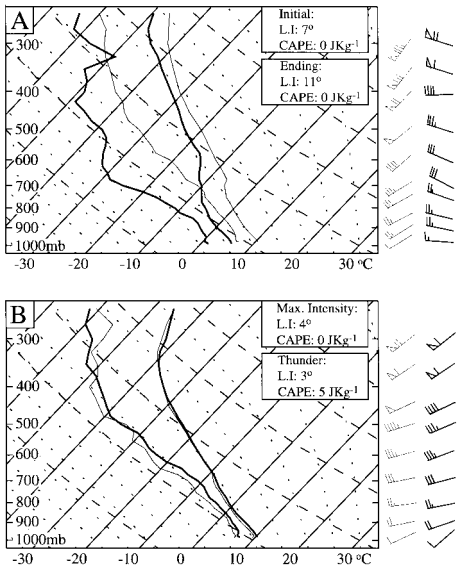

FIG. 13. (a) Mean Buffalo soundings for the initial (thin lines) and ending stages (bold lines). (b) Same as (a) but for maximum intensity (thin lines) and thunder times (bold lines).

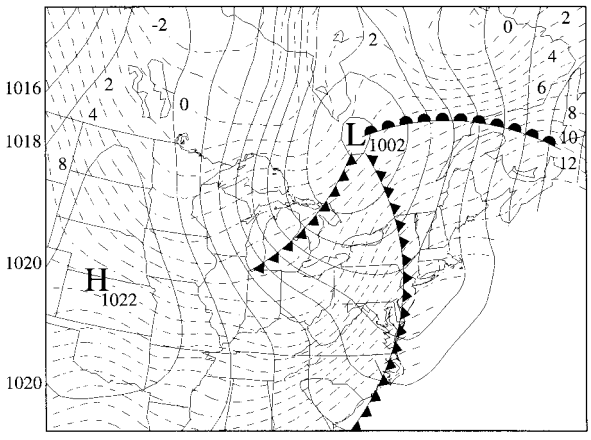

FIG. 14. Mean surface pressure (mb) and temperature (°C) analysis of initial stage events. A subjective analysis of key synoptic features is overlain.

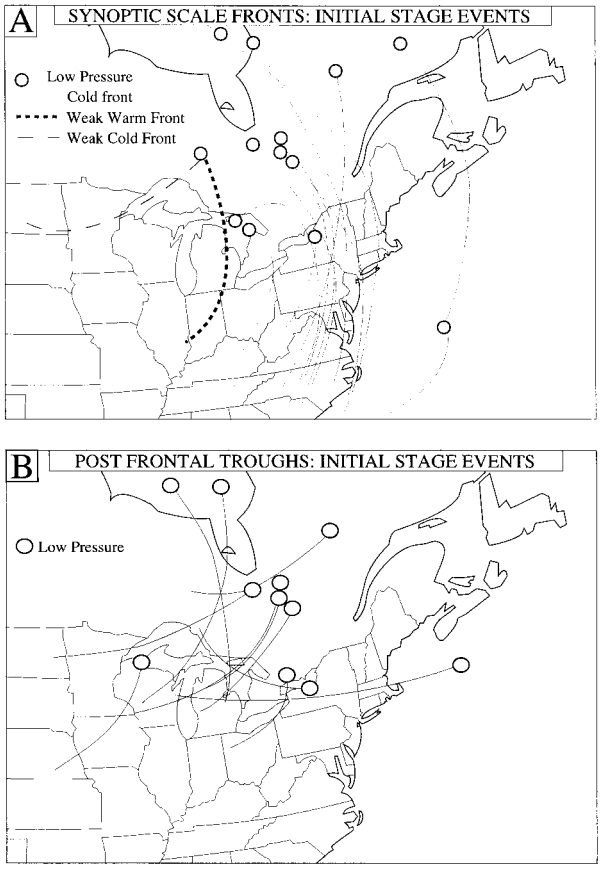

FIG. 15. (a) Location of synoptic-scale fronts for all the events contained in the mean initial stage analyses. (b) Same as (a) but for postfrontal troughs.

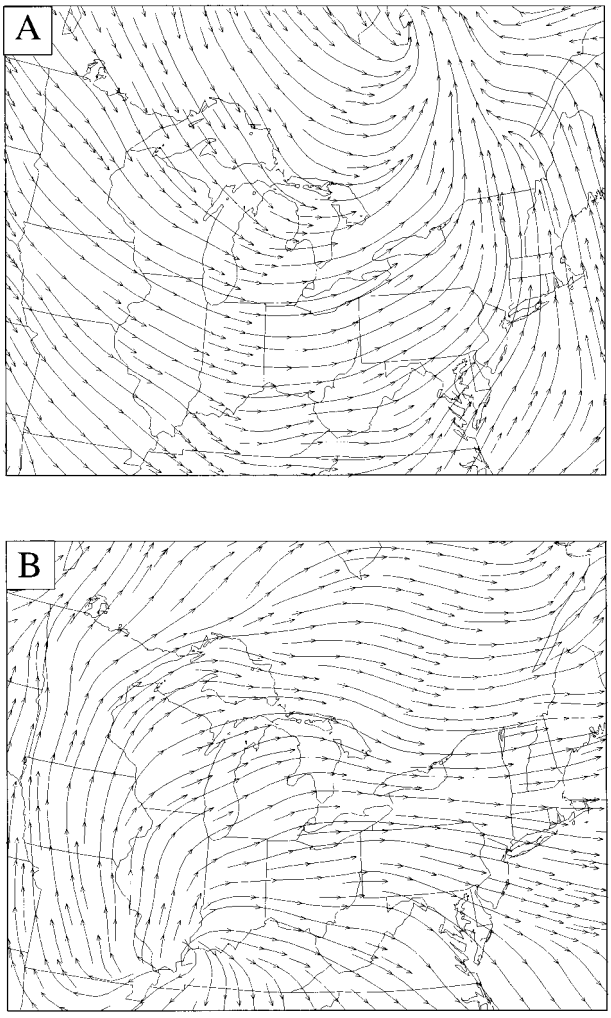

FIG. 16. Mean surface streamline analysis of the (a) initial stage and (b) ending stage. Note the change from cyclonic to anticyclonic flow from the initial to ending stage.

these precipitation events. Because the vertical shear profile is dynamically unfavorable for producing other modes of convection like conditional symmetric instability (CSI), a logical hypothesis is that the local modification of air by Lake Erie induces moist convection. Therefore, a procedure was devised to estimate the temperature and dewpoint of air parcels modified in transit over the lake by using the following simple approximations:

$$T = (\text{Tlake} + \text{TBuf})/2 \quad (1)$$

and

$$D = (\text{Dlake} + \text{DBuf})/2, \quad (2)$$

where TBuf and DBuf are the mean values of Buffalo airport temperature and dewpoint and Tlake and Dlake are the mean values of lake water temperature and dewpoint. Dlake was obtained using the following method: First, the ratio R of the temperature lapse rate in the 975- to 950-mb layer to the lake surface to 950-mb layer was calculated:

TABLE 2. Convective indices for the initial, maximum intensity, ending, and thunder mean soundings at Buffalo, New York, calculated by SHARP. Indices are shown for the unmodified Buffalo sounding and the two modified versions. Note the marked decrease in stability that occurs after inserting the lake surface and lake air temperature and dewpoint values.

	Time							
	Initial		Ending		Max int.		Thunder	
Convective index:	LI	CAPE	LI	CAPE	LI	CAPE	LI	CAPE
Buffalo Airport	7	0	11	0	4	0	3	5
Lake Erie surface	1	415	5	369	−5	1222	−5	1289
Lake Erie air	4	130	8	89	0	394	−1	465

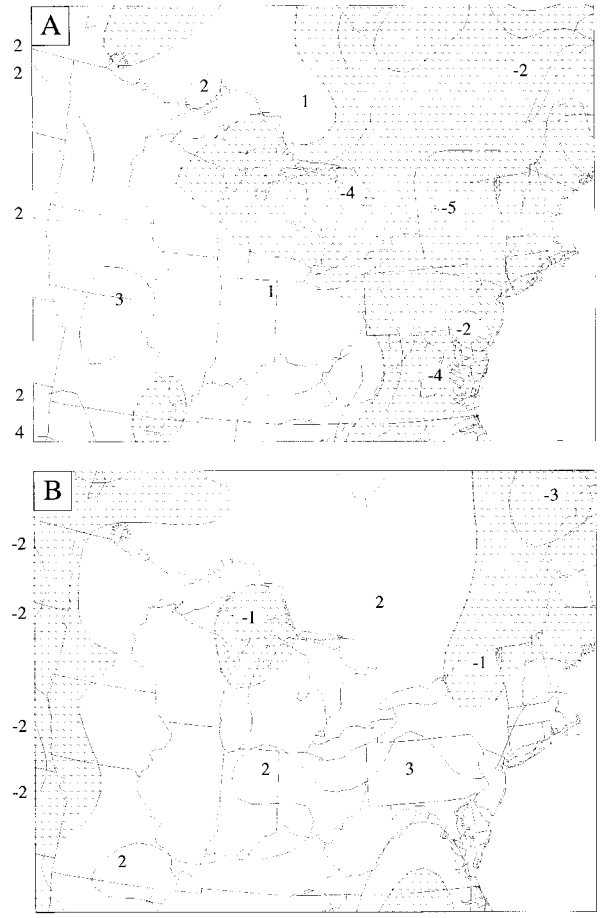

FIG. 17. (a) Mean surface moisture divergence (contour interval 2 $\times 10^{-7}$ s^{-1}) for the initial stage. (b) Same as (a) but for the ending stage. Stippling denotes regions of convergence.

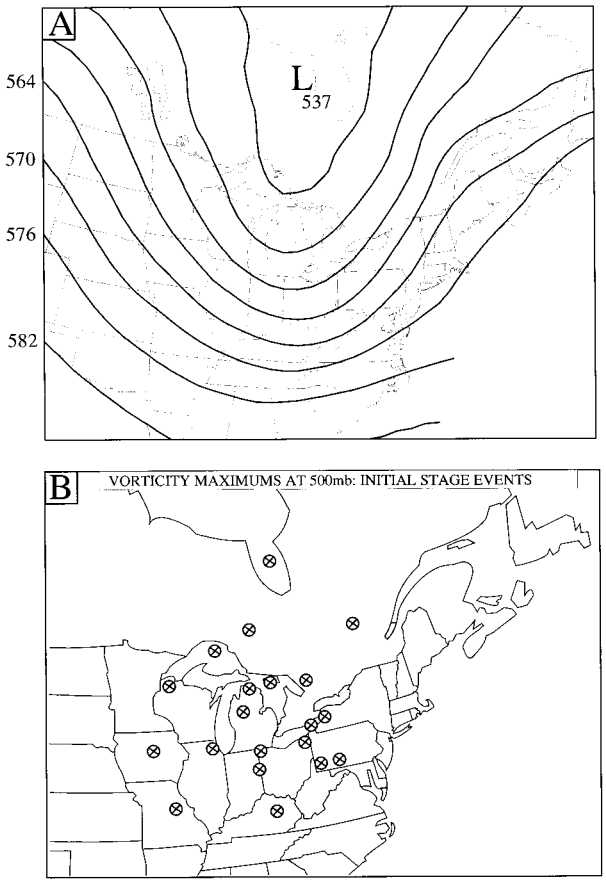

FIG. 18. (a) Initial stage 500-mb mean height analysis (dam). (b) Location of 500-mb vorticity maxima for all the events contained in the initial stage. For events with two maxima, both are shown.

$$R = \frac{\text{T975} - \text{T950}}{\text{Tlake} - \text{T950}}. \quad (3)$$

Afterward, the lake surface dewpoint (Dlake) was found by assuming that the ratio (3) also applies for the dewpoint,[10] that is,

$$R = \frac{\text{D975} - \text{D950}}{\text{Dlake} - \text{D950}}. \quad (4)$$

The convective instability of the unmodified mean Buffalo sounding and the two modified versions (lake surface and air over the lake) is summarized in Table 2. Although this estimation technique is crude, these lake air estimates nearly match several events where ship observations of temperature and dewpoint were available. Furthermore, in using these ''lake Erie air'' values as input to the NWS SHARP program, it was found that the observed mean maximum echo top (20 900 ft) falls between what SHARP produces for the cloud top (27 214 ft) and equilibrium level (18 407 ft).

d. Mean large-scale environment

1) INITIAL STAGE

Figure 14 shows the mean analysis of surface temperature and pressure for the initial stage of the lake-effect rain events. Overlaid are subjective depictions of the synoptic-scale fronts and attendant postfrontal trough positions. In addition, the positions of the primary surface lows, attendant synoptic-scale cold fronts, and troughs for each initial stage event included in the mean analysis are shown in Figs. 15a,b. Together, Figs. 14 and 15a clearly indicate that the start of a typical event occurs shortly after the passage of a low and attendant cold front. In addition, Fig. 15b indicates that postfrontal troughs are often found west of Lake Erie

[10] Technically, the dewpoint of the lake surface is equal to the temperature of the lake surface. This is true because at the lake water interface, the vapor pressure is equal to the saturation vapor pressure of the water temperature. However, using the skin temperature as the skin dewpoint in SHARP yielded cloud-top values that were much higher than what was observed. This probably occurs because the near-lake surface vapor pressure gradient is greater than the near-surface temperature gradient.

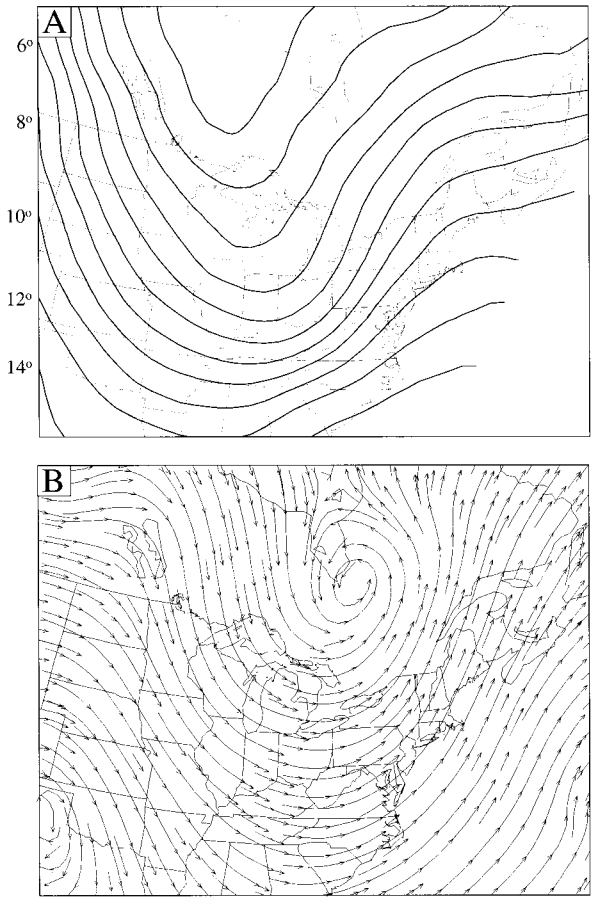

FIG. 19. (a) Initial stage 850-mb mean analysis for (a) temperature (°C) and (b) streamlines.

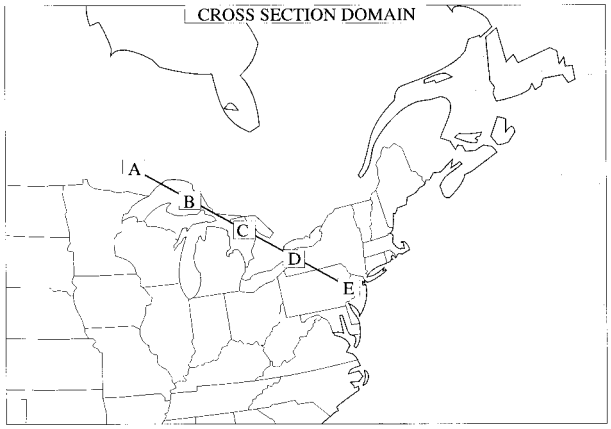

FIG. 20. Cross-sectional domain for the initial, ending, maximum intensity, and thunder mean upper-air analyses. Letters *A–E* depict cross section location points used in Figs. 21, 24, and 30.

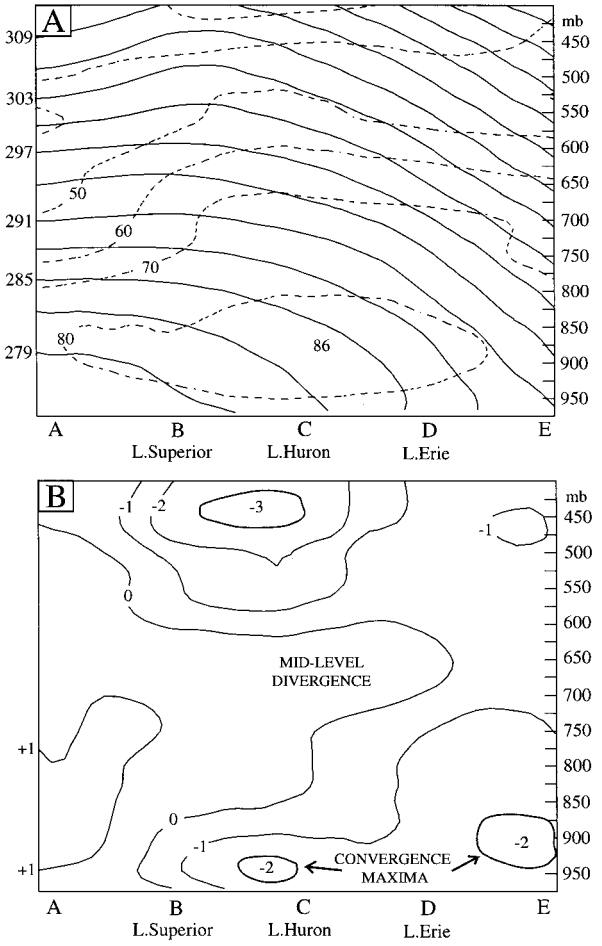

FIG. 21. Mean initial stage cross section. (a) Vertical cross section of potential temperature (K, solid) and relative humidity (%, dashed). Location points *A–E* are shown along bottom (see Fig. 20). (b) Same as (a) except divergence shown (1×10^{-5} s^{-1}). Positive (negative) values denote divergence (convergence).

at the onset of the lake-effect events. Not surprisingly, the positions of the primary surface pressure features are very similar to those noted by Wiggin (1950) for heavy lake-effect snow events in western New York.

Subtle examples of how fluxes from all five Great Lakes alter the thermodynamic environment are shown in Fig. 14. The figure shows a weak thermal ridge from Lake Superior southeast to Michigan while a cold trough curves southeast from Minnesota to southern Ohio, appearing to circumvent the western Great Lakes. Similar patterns were found by Sousounis and Fritsch (1994) in their analysis of a wintertime lake-effect snow event.

A surface streamline analysis (Fig. 16a) shows southwesterly surface flow across the eastern Lakes region, veering to a northwesterly direction in the western Great Lakes. The wind shift across the central Lakes apparently marks the mean location of the trailing surface trough (see Figs. 14 and 15b). An analysis of the mean surface moisture convergence (Fig. 17a) indicates a convergence pattern over the Great Lakes and East Coast. The convergence east of the lakes is likely associated with the mean position of the synoptic low and cold front. The convergence over the lakes is probably a

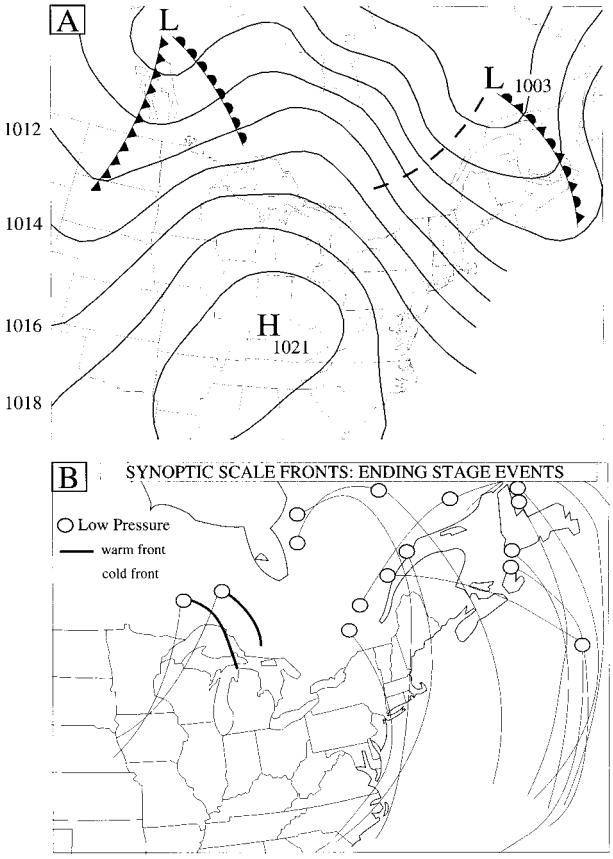

FIG. 22. (a) Mean surface pressure (mb) analysis for the ending stage. A subjective analysis of key synoptic features is overlain. (b) Location of synoptic-scale fronts for each ending stage event.

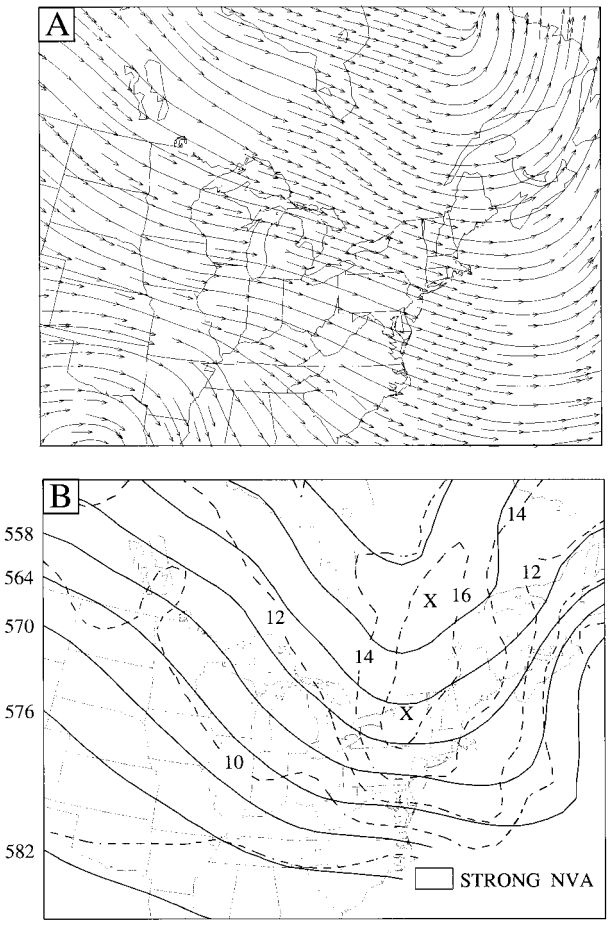

FIG. 23. (a) Mean ending stage analysis for (a) 850-mb streamlines. (b) The 500-mb heights and absolute vorticity. Heights (dam) are solid contours while dashed lines represent vorticity isopleths (1×10^{-5} s^{-1}). The region of strongest negative vorticity advection (NVA) is shaded.

reflection of the postfrontal trough over the lakes as well as the frictional effects of the cyclonic flow (cf. Figs. 14a and 17a). The postfrontal surface trough is likely a signature of the mean position of a transient synoptic-scale disturbance whose amplitude is enhanced by the sensible and latent effects of the lakes. Moisture divergence from the synoptic-scale subsidence covers the region southwest of the lakes.

The mean anaylsis at 500 mb depicts a low center near James Bay, Canada (Fig. 18a). The vertical stacking of the low (cf. Figs. 14 and 18a) indicates that there is little vertical directional shear and that the synoptic frontal system exiting the Great Lakes is occluding. The 500-mb low position (Fig. 18a) matches Wiggin's (1950) requisite conditions for prolonged lake-effect snows at the eastern end of Lake Erie. Also, a depiction of 500-mb vorticity maxima in Fig. 18b for each initial stage event shows a clustering of maxima mostly to the west of Lake Erie. This places Lake Erie in a region of positive vorticity advection (PVA), a favorable location for large-scale ascent.

The thermodynamic structure aloft is similar to the surface pattern in regard to the trend toward colder and drier air northwest of the Atlantic seaboard. At 850 mb, a thermal trough extends from west of Hudson Bay southward to the western Great Lakes (Fig. 19a) while a dry tongue in the dewpoint field stretches from west of Hudson Bay south into the Mississippi Valley (not shown). In addition, west to southwesterly cyclonic flow along the long axis of Lake Erie exists at 850 mb (Fig. 19b).

A cross section (Fig. 20) of relative humidity and potential temperature (Fig. 21a) shows an enhanced depth of moist (high relative humidity) air across the Great Lakes, with its greatest depth over the central Great Lakes. The lakes region is clearly in the post-cold-frontal air as noted by the concave curvature of the theta surfaces (Fig. 21a). Notice, however, that below 850 mb the atmosphere is least stable across the eastern half of the Great Lakes.

The high relative humidity values across the eastern portion of the Great Lakes are likely a product of synoptic-scale ascent. Such large-scale ascent is inferred by deep convergence present to the east of Lake Erie (Fig.

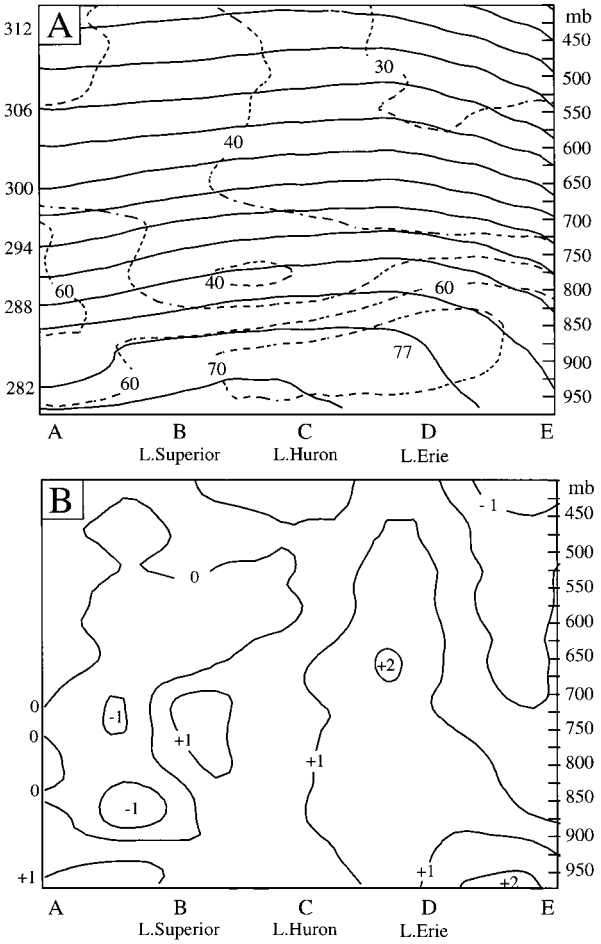

FIG. 24. Mean ending stage cross section. (a) Vertical cross section of potential temperature (K, solid) and relative humidity (%, dashed). Location points *A–E* are shown along bottom (see Fig. 20). (b) Same as (a) except divergence shown (1×10^{-5} s^{-1}). Positive (negative) values denote divergence (convergence).

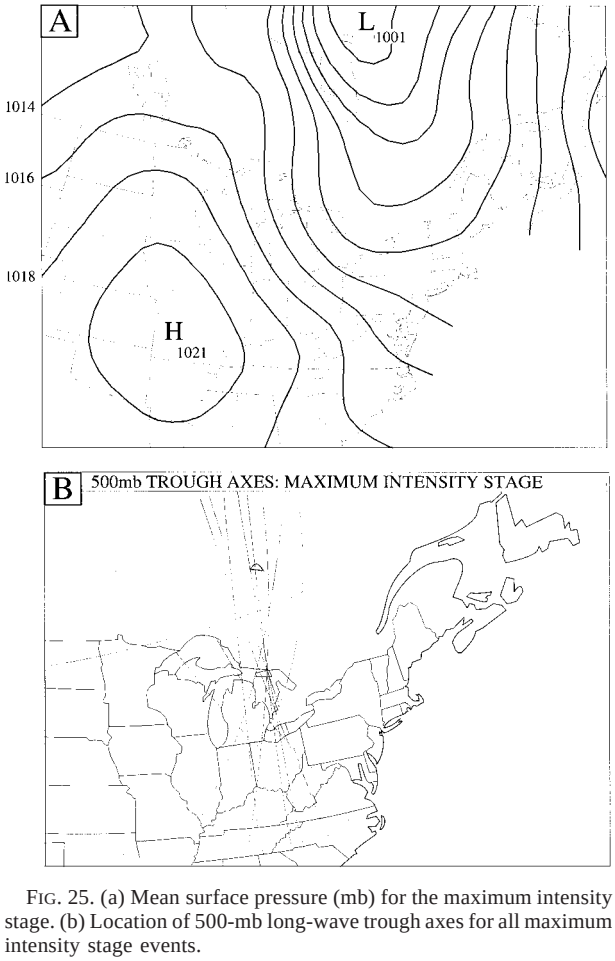

FIG. 25. (a) Mean surface pressure (mb) for the maximum intensity stage. (b) Location of 500-mb long-wave trough axes for all maximum intensity stage events.

21b). Farther west, low-level convergence overlain by middle tropospheric divergence indicates a much shallower tropospheric circulation.

2) ENDING STAGE

The mean analyses of the ending stage depicts a regime that is much different from the initial stage. Surface systems have shifted toward the east with the James Bay low now over the Gulf of Saint Lawrence and the synoptic high now over the Ohio Valley (cf. Figs. 22, 14, and 15a). Surface pressures have risen 5–10 mb over the Great Lakes while the flow has turned northwesterly and anticyclonic (Fig. 16b).

A manifestation of the anticyclonic northwest surface flow is found in the moisture divergence pattern. Surface moisture divergence covers the Great Lakes region in contrast to the convergence pattern of the initial stage (cf. Figs. 17a,b). The surface moisture divergence and the reduced fetch length from the northwest flow contribute to the termination of the lake-effect precipitation. Lingering effects of lake-modified air, however, are apparent in the surface temperature and dewpoint analyses where thermal and moist ridges persist (not shown).

Noticeable differences between the initial and ending stages are also evident in the mean upper-air analyses. Flow at 850 mb has become northwest and anticyclonic (cf. Figs. 23a and 19b). Meanwhile, the James Bay closed low at 500 mb has moved well northeast of its previous position and the 500-mb trough axis now lies east of the Great Lakes. This places Lake Erie in a region of pronounced negative vorticity advection (NVA) (Fig. 23b). Compared to initial stage values, tropospheric relative humidity levels have diminished in both depth and magnitude across the Great Lakes. This is clearly evident from a comparison of the initial and ending stage cross sections through the lakes region (cf. Figs 24a and 21a). The lowering of relative humidity values is attributed to synoptic-scale subsidence that occurs after the passage of the 500-mb trough axis and vorticity maximum. In agreement with this interpretation, Fig. 24b shows a deep layer of divergence over the eastern portion of the lakes region.

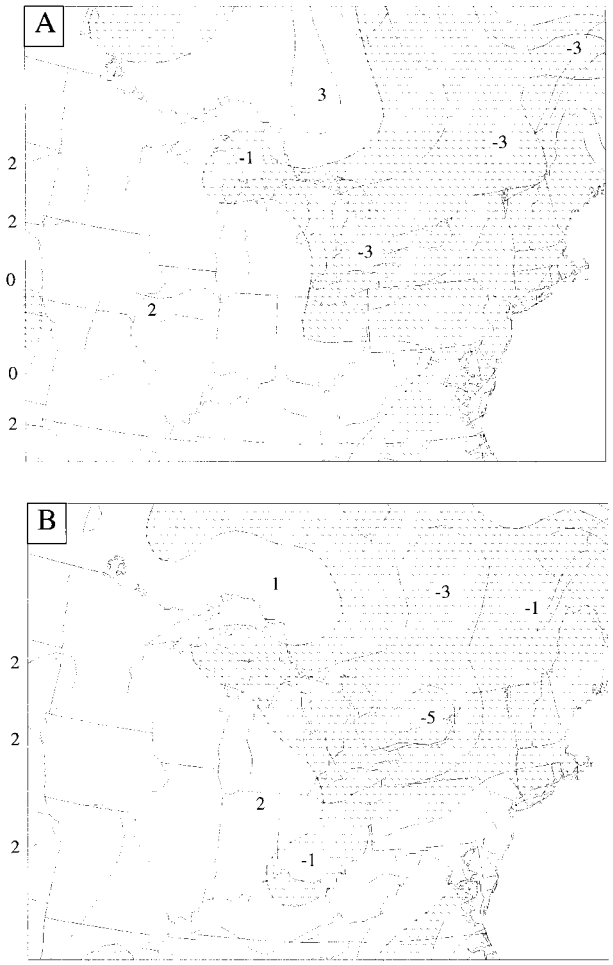

FIG. 26. (a) Mean surface moisture divergence (contour interval 2 $\times 10^{-7}$ s^{-1}) for the maximum intensity stage. (b) Same as (a) but for thunder events. Stippling denotes regions of convergence.

3) MAXIMUM INTENSITY STAGE

The surface analyses of the maximum intensity stage, where echo tops have achieved their greatest heights, is quite similar to the initial stage. At the surface, a pressure trough extends from northeast Ontario province southwest to the eastern Great Lakes (Fig. 25a). Enhanced surface moisture convergence is noted in Fig. 26a over Lake Erie. Also noted, is an apparent surface equivalent potential temperature perturbation that has developed over the Great Lakes region (Figs. 27a–c). The perturbation is likely caused by sensible and latent heat exchanges from all five Great Lakes to the overlying atmosphere. A hand-drawn ''perturbed'' field of equivalent potential temperature (Fig. 27c) was constructed by subtracting a subjectively smoothed analysis from the actual analysis.

Likewise, the mean upper-air analyses (not shown) are very similar to the initial stage. A broad trough extends through the depth of the troposphere from Hudson Bay to the Great Lakes. This pattern is evident at 500 mb where the mean trough axis lies from Hudson Bay to the central Great Lakes. A depiction of the 500-mb trough axis for each event shows a cluster of trough axes just west of Lake Erie (Fig. 25b), placing the eastern Great Lakes in a favorable region of synoptic ascent.

4) THUNDER EVENTS

For the most part, the mean surface and upper-air analyses for thunder events are similar to the maximum intensity and initial stages. Figure 28 depicts the synoptic surface fronts and trailing surface troughs for each thunder event contained in the mean analyses. The clustering of surface troughs in the vicinity of the eastern Lakes agrees with Moore and Orville (1990), who found that cloud-to-ground lightning activity for Lake Erie and Ontario effect storms is most frequent near the passage of a surface trough.

Of special note for thunder events is a large component of ageostrophic wind and a deep layer of exceptionally high relative humidity over the Lake Erie region. The ageostrophic flow is inferred by comparing the west-northwest geostrophic flow of the surface pressure field (Fig. 29a) to the west-southwest streamline analysis (Fig. 29b) over eastern Lake Erie. This highly ageostrophic, cyclonic flow enhances surface convergence and subsequent boundary layer ascent, as depicted by the surface moisture convergence pattern in Fig. 26b.

In the cross sections, the vertical axis of the highest humidity layer has shifted eastward from its position over the central lakes region at the initial stage time to a location almost directly over Lake Erie (cf. Figs. 21a and 30a). Note also that the greater than 80% layer is considerably deeper than at the onset of the lake-effect event and that the peak value lies in the low-level convergence–midlevel divergence couplet (cf. Figs. 30a,b).

4. Comparison to lake-effect snow events

a. Similarities

There are many similarities between lake-effect rain and snow events. Fundamentally, both are driven by convective sensible and latent heat exchanges from the lake to the free atmosphere. Not surprisingly, very similar synoptic patterns are visible during both lake-effect snow and rain events: 1) cold advection across the Great Lakes and a cold front stretching north–south along the East Coast, 2) a deep layer of westerly flow along the long axis of Lake Erie with surface and 500-mb lows north of the Great Lakes, 3) a postfrontal trough trailing over the Great Lakes, and 4) a surface high over the central Plains [see Niziol (1987) for the synoptic conditions favorable for lake-effect snow].

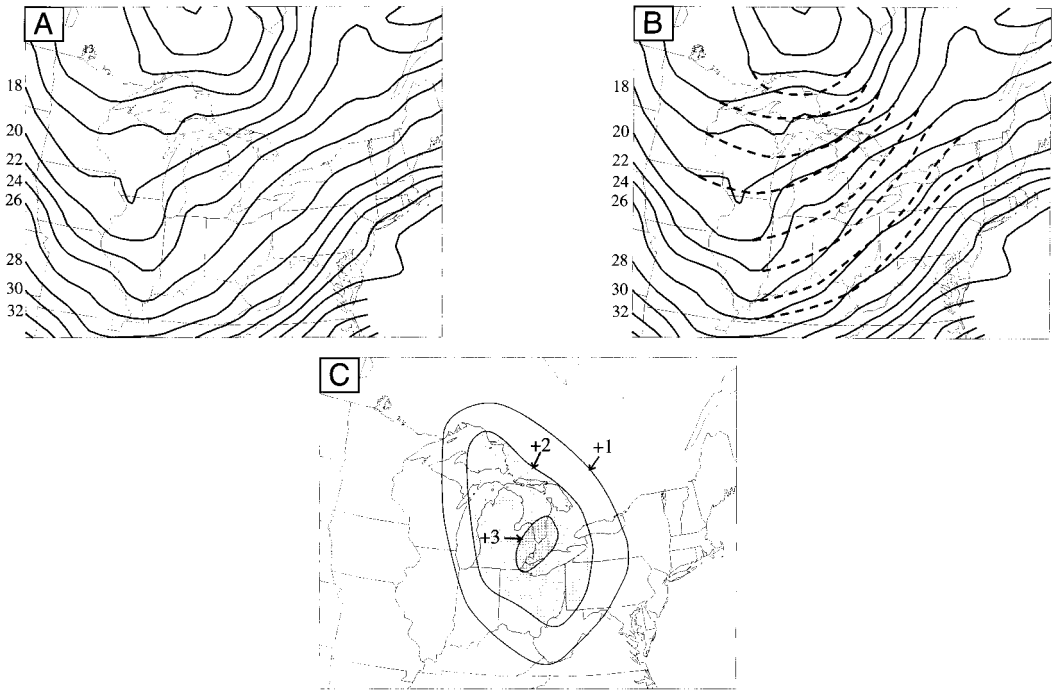

FIG. 27. (a) Mean equivalent potential temperature of the maximum intensity stage. (b) A subjectively smoothed analysis eliminating the kink over the Great Lakes overlays the equivalent potential temperature of (a). (c) A hand-drawn estimate of the equivalent potential temperature perturbation induced by all five Great Lakes. All values are in degrees Celsius.

b. Differences

Since all lake-effect precipitation begins in the clouds as snow, the thermal profile between the precipitation echo top and the surface ultimately determines whether precipitation reaches the ground as rain or snow. Thus, in rain events, the temperature of the boundary layer must exceed 0°C through a sufficient depth to turn snow to rain. In addition to this obvious difference, lower-tropospheric stability also differs between lake-effect rain and lake-effect snow cases. For example, the extreme lower tropospheric instabilities often observed during lake-effect snow are rarely observed in lake-effect rain events. This is illustrated in Fig. 31, which compares the mean Buffalo sounding at the time of maximum intensity of lake-effect rain events to the mean sounding at the time of maximum intensity for 10 lake-effect snow events.[11]

While the magnitude of low-level instability is less for most rain events, the depth of the conditionally unstable layer is much greater. This is clearly shown in Fig. 31 where maximum possible instabilities for both rain and snow soundings are shown. Assuming the lake surface to be the level of free convection, a parcel for the rain sounding rises to an altitude of 300 mb compared to 500 mb for the snow sounding. Directly related to the deeper layer of instability is the frequent absence of a subsidence inversion typically present during lake-effect snow events (Niziol 1987). Inspection of the Buffalo sounding during the maximum intensity period of 16 lake-effect rain events revealed that only four had subsidence inversions.

The frequent absence of subsidence inversions in lake-effect rain events implies the presence of large-scale ascent across the eastern Great Lakes. For rain events, this was typically indicated by an approaching short wave and attendant surface trough from the west. The adiabatic ascent associated with the approaching trough aids in lifting the inversion while simultaneously raising the tropospheric relative humidity. With higher environmental humidity present, dry air entrainment is reduced, allowing lake-modified parcels to experience moist-adiabatic ascent through a deeper layer. This, combined with the fact that moist adiabatic ascent approaches dry ascent in colder environments, may explain why many lake-effect rain events (in contrast to snow) occur when the lake surface to 850-mb temperature difference is between moist and dry adiabatic.

Another consequence of the high relative humidity is the widespread cloud cover that typically accompanies rain events. In contrast to snow events, where midtropospheric subsidence often allows for a clear view of

[11] The events were selected from the list of 1995–96 lake-effect snow events cataloged by the NWS Buffalo Forecast Office. Sounding selection followed the same procedure outlined in section 2.

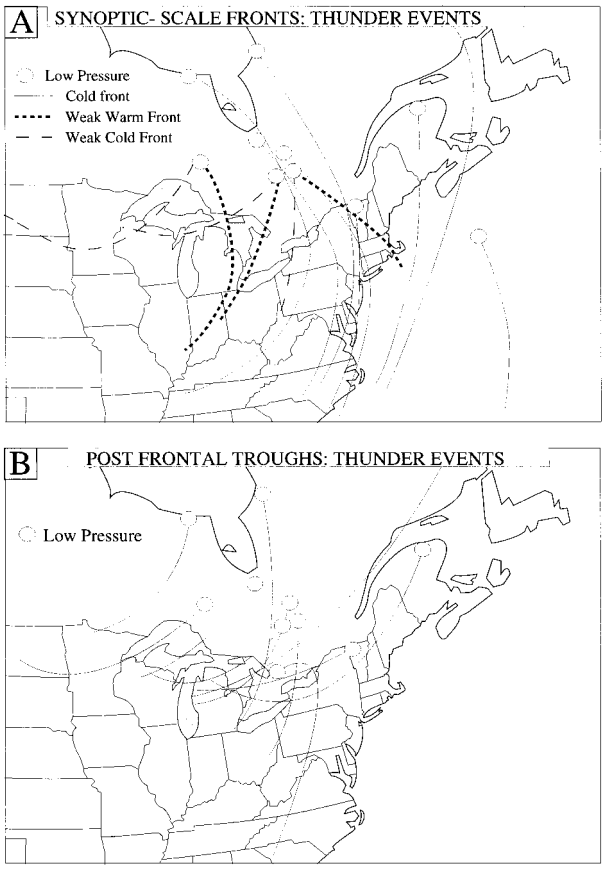

FIG. 28. (a) Location of synoptic-scale fronts for all the events contained in the mean thunder analysis. Open dots mark the location of low pressure centers while cold fronts are depicted as thin lines. Weak warm fronts are depicted as thick dashed lines while weak cold fronts are shown as thin dashed lines. (b) Postfrontal trough positions for all the thunder events.

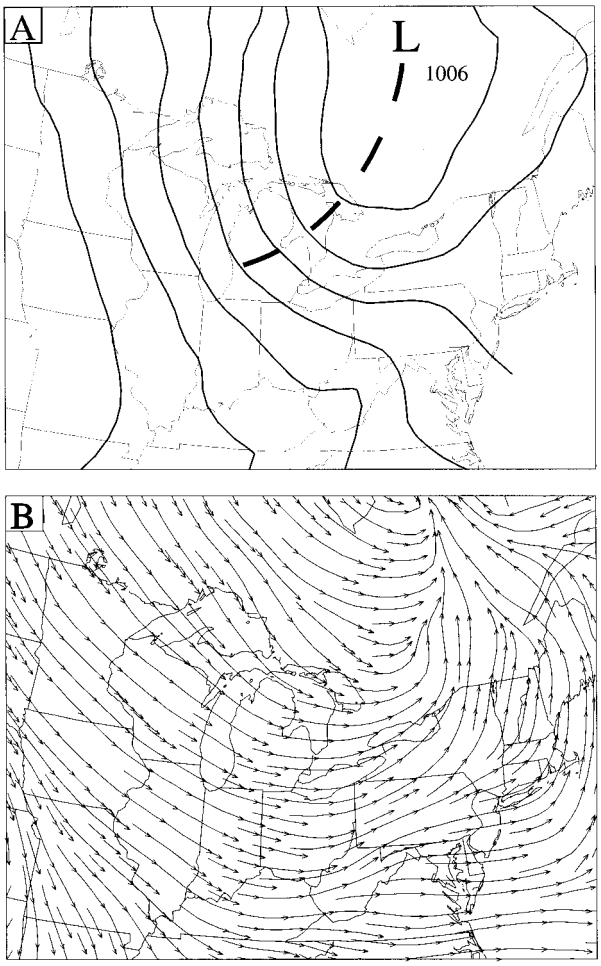

FIG. 29. Mean analyses for lake-effect thunder events: (a) Surface pressure with trough indicated over the lakes and (b) surface streamlines. Note the large ageostrophic component of the wind over the eastern Great Lakes as indicated by the difference in geostrophic (inferred by the pressure analysis) wind in (a) and real wind in (b).

lake-forced clouds, satellite detection of lake-effect rain can be particularly difficult. Thus, the recently completed study of lake-effect frequency from visible satellite observations by Kristovich (1995) may be a significant underestimation of the total population of early season lake-effect events.

The weak inversions during lake-effect rain events also appear to contribute to the production of much deeper clouds than those observed during snow events. For example, the mean maximum intensity stage echo top of 20 900 ft is considerably higher than the typical 5–15 000 ft observed during lake-effect snow events. These higher cloud tops would suggest that the steering flow for lake-effect rain may be better approximated by the mean 850–700-mb wind rather than the 850-mb wind vector as is typically used for pinpointing the location of lake-effect snow bands (Niziol 1987).

5. Summary and conclusions

Based on the examination of radar-observed precipitation around Lake Erie, it was found that lake-effect precipitation occurs throughout the autumn. Precipitation is typically in the form of rain during September and October, both rain and snow during the first 10 days of November, and almost exclusively snow thereafter. The frequency of lake-effect precipitation was measured by compiling both lake-effect days and lake-effect events. To qualify as a lake-effect event, precipitation must be observed downwind of Lake Erie for a minimum of six consecutive hours while there is cold advection over the lake. A lake-effect event differs from a lake-effect day in that an event may span several days. A tally of all autumnal lake-effect days from 1988 through 1994 indicated that October was the most active lake-effect month (with 53 days), followed by November (47 days), and then September (22 days). A tally of Lake Erie–effect events covering this same time period shows similar result with a slight maximum in November. An analysis of long-term regional precipitation climatologies confirms the radar study and indicates that

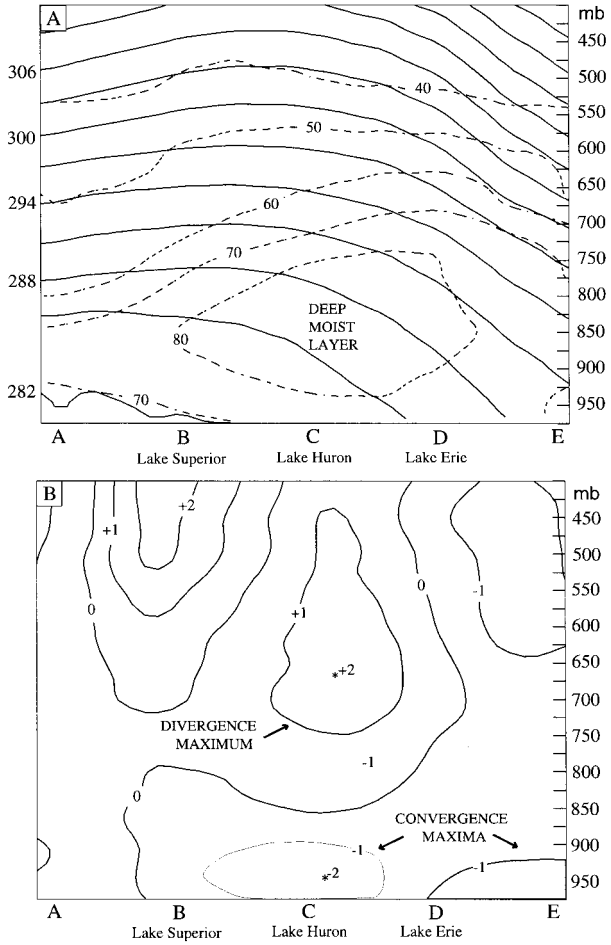

FIG. 30. Mean cross section for lake-effect thunder events. (a) Vertical cross section of potential temperature (K, solid) and relative humidity (%, dashed). Location points *A–E* are shown along bottom (see Fig. 20). (b) Same as (a) except divergence is shown (1×10^{-5} s^{-1}). Positive (negative) values denote divergence (convergence).

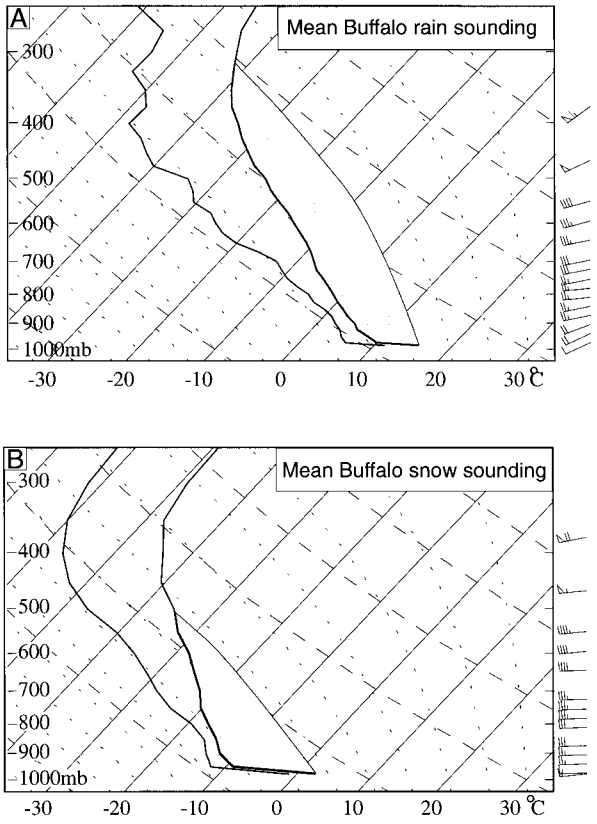

FIG. 31. (a) Mean Buffalo rain sounding at the time of maximum intensity. (b) Mean Buffalo snow sounding at the time of maximum intensity. Maximum possible CAPE is shaded for both soundings. Lake temperature and dewpoint are used for surface values.

lake-effect precipitation begins in earnest by September and reaches a maximum during late fall and early winter. While the frequency of precipitation may be greater in the winter, the climatological precipitation patterns suggest that the peak in lake-effect precipitation amount occurs in the autumn.

The earlier maximum in precipitation amount agrees with the late September to mid-October frequency peak of thunder events. While October had the greatest number of lake-effect thunder events, September had the highest percentage of thunder per lake-effect event with thunder observed in over 40% of all September events. Increasing tropospheric stabilities likely caused the significant decline of lake-effect thunder events in November.

Examination of the diurnal distribution of maximum echo tops revealed that the peak in lake-effect intensity occurs during the afternoon and evening hours. In particular, the greatest number of maximum echo tops for all rain events was observed between 0000 and 0500 UTC while the greatest number of thunder observations occurred between 1800 and 2300 UTC. Moreover, the afternoon into evening maximum period was also noted in the distribution of observed precipitation totals during the nine ''heavy rain'' events. This particular diurnal cycle suggests that in many instances the low-level destabilization induced by solar heating is an important supplement to the heat and moisture fluxes from the lake.

An estimate of the mean large-scale environment during lake-effect rain was constructed by averaging the environments of the individual events at certain stages in their life cycles. Overall, the mean lake-effect rain analyses show considerable similarities to snow events. The similarities are most notable in the general position of synoptic-scale features. Of particular note is the presence of a surface and upper-air low pressure center near James Bay, Canada, with cold advection present across the Great Lakes and Northeast. Differences between rain and snow environments are manifested primarily in the thermodynamic profile of the lower to middle troposphere. Compared to most lake-effect snow events, the magnitude of the low-level instability in rain events is

less while the depth of the conditionally unstable layer is much greater.

Acknowledgments. The authors would like to thank the Weather Communications Group at Penn State University for their technical support throughout the project. A special thanks to Fred Gadomski whose advice and wisdom helped shape this paper. Also acknowledged are the staffs of the National Weather Service at Buffalo, New York, and State College, Pennsylvania. Particularly helpful were Steve McLaughlin and Tom Niziol. This research was supported by the meteorology department at Penn State University. Other financial supporters were COMET under subaward S95-56772 and the National Science Foundation under Grants ATM 92-22017 and 95-28853.

REFERENCES

Ballentine, R. J., G. P. Byrd, and T. A. Niziol, 1993: An operational forecast model for lake-effect snowstorms. Preprints, *13th Conf. on Weather Analysis and Forecasting,* Vienna, VA, Amer. Meteor. Soc., 154–157.

Barnes, S. L., 1964: A technique for maximizing detail in numerical weather map analysis. *J. Appl. Meteor.,* **3,** 396–409.

Beebe, R. G., 1952: The distribution of summer showers over a small area. *Mon. Wea. Rev.,* **80,** 95–98.

Byrd, G. P., R. A. Anstett, J. E. Heim, and D. M. Usinski, 1991: Mobile sounding observations of lake-effect snowbands in western and central New York. *Mon. Wea. Rev.,* **119,** 2323–2332.

Changnon, S. A., 1988: Climatology of thunder events in the conterminous United States. Part II: Spatial aspects. *J. Climate,* **1,** 399–405.

——, and D. M. Jones, 1972: Review of the influences of the Great Lakes on weather. *Water Resour. Res.,* **8,** 360–371.

Dockus, D. A., 1985: Lake effect snow forecasting in the computer age. *Natl. Wea. Dig.,* **10,** 5–19.

Hart, J. A., and J. Korotky, 1991: The SHARP Workstation—v1.50. A skew T-hodograph analysis and research program for the IBM and compatible PC. User's Manual. NOAA/NWS Forecast Office, Charleston, WV, 62 pp. [Available from NOAA/NWS, 400 Parkway Road, Charleston, WV 25309.]

Hill, J. D., 1971: Snow squalls in the lee of Lakes Erie and Ontario. NOAA Tech. Memo. NWS ER-43, 20 pp. [NTIS COM-72-00959.]

Hirschberg, P. A., and J. M. Fritsch, 1991: Tropopause undulations and the development of extratropical cyclones. Part II: Diagnostic analysis and conceptual model. *Mon. Wea. Rev.,* **119,** 518–550.

Hjelmfelt, M., 1990: Numerical study of the influence of environmental conditions on lake-effect snowstorms on Lake Michigan. *Mon. Wea. Rev.,* **118,** 138–150.

Holyroyd, E. W., III, 1971: Lake effect cloud bands as seen from weather satellites. *J. Atmos. Sci.,* **28,** 1165–1170.

Kelly, R. D., 1984: Horizontal roll and boundary-layer interrelationships observed over Lake Michigan. *J. Atmos. Sci.,* **41,** 1816–1826.

Kolker, B., 1978: Current forecast procedures for lake effect snow in western New York especially related to the 1976–1977, and 1977–1978 winters. *Proc. 25th Annual Eastern Snow Conf.,* Hanover, NH, U.S. Army, 17–35.

Kristovich, D. A. R., and R. A. Steve, 1995: A satellite study of cloud-band frequencies over the Great Lakes. *J. Appl. Meteor.,* **34**, 2083–2090.

Lavoie, R. L., 1972: A mesoscale numerical model of lake-effect storms. *J. Atmos. Sci.,* **29,** 1025–1040.

Lenschow, D. H., 1973: Two examples of planetary boundary layer modification over the Great Lakes. *J. Atmos. Sci.,* **30,** 568–581.

Moore, P. K., and R. E. Orville, 1990: Lightning characteristics in lake effect thunderstorms. *Mon. Wea. Rev.,* **118,** 1767–1782.

Mundschenk, R. R., 1993: An analysis of a lake-enhanced rain event off Lake Erie. Tech. Attachment ERTA NO. 93-9A, NOAA/NWS, Buffalo, NY, 1–17. [Available from NOAA/NWS, 587 Aero Drive, Buffalo, NY 14225.]

Niziol, T. A., 1987: Operational forecasting of lake effect snow in western and central New York. *Wea. Forecasting,* **2,** 310–321.

——, W. R Snyder, and J. S. Waldstreicher, 1995: Winter weather forecasting throughout the eastern United States. Part IV: Lake effect snow. *Wea. Forecasting,* **10,** 61–77.

Passarelli, R. E., Jr., and R. R. Braham, 1981: The role of the winter land breeze in the formation of Great Lakes snowstorms. *Bull. Amer. Meteor. Soc.,* **62,** 482–491.

Sousounis, P. J., and J. M. Fritsch, 1994: Lake-aggregate mesoscale disturbances. Part II: A case study of the effects on regional and synoptic-scale weather systems. *Bull. Amer. Meteor. Soc.,* **75,** 1793–1811.

Wiggin, B. L., 1950: Great snowstorms of the Great Lakes. *Weatherwise,* **3,** 123–126